RSC Advances

This article can be cited before page numbers have been issued, to do this please use: Y. Wang, C. Hou, Y. Zhang and M. Liu, *RSC Adv.*, 2015, DOI: 10.1039/C5RA20996J.

ROYAL SOCIETY OF CHEMISTRY

www.rsc.org/advances

View Article Online
DOI: 10.1039/C5RA20996J

Magnetic Fe_3O_4@MOFs decorated graphene nanocomposites as novel electrochemical sensor for ultrasensitive detection of dopamine

Yang Wang, Yun Zhang *, Chen Hou, Mingzhu Liu*

State Key Laboratory of Applied Organic Chemistry, Key Laboratory of Nonferrous Metal Chemistry and Resources Utilization of Gansu Province, College of Chemistry and Chemical Engineering, College of Resources and Environment, Institute of Biochemical Engineering &Environmental Technology, Lanzhou University, Lanzhou 730000, China

Abstract

A novel hybrid nanocomposite of magnetic Fe_3O_4@ZIF-8 (zeolitic imidazolate framework-8 coated Fe_3O_4 nanocomposites denoted as Fe_3O_4@ZIF-8) decorated RGO (reduced graphite oxide) was prepared by a simple method for the first time and denoted as Fe_3O_4@ZIF-8/RGO. After the Fe_3O_4/RGO was formed by solvothermal approach, the MOFs (ZIF-8) was coated on the surface of Fe_3O_4 to get the Fe_3O_4@ZIF-8/RGO nanocomposite. The resulted Fe_3O_4@ZIF-8/RGO nanocomposite was characterized by means of the transmission electron microscope (TEM), scanning electron microscopy (SEM), Fourier transform infrared spectra (FT-IR), X-ray diffraction spectrometry (XRD), X-ray photoelectron (XPS), and vibrating sample magnetometer (VSM). This nanocomposite was modified on the glassy carbon electrode to fabricate biosensor which used to electrochemical determination for dopamine (DA) in phosphate buffer solution. The results demonstrated the fabricated

*Corresponding author. Fax: 86-931-8912113; *E-mail address*: zhangyun@lzu.edu.cn (Y. Zhang)
*Corresponding author. Fax: 86-931-8912582; *E-mail address*: mzliu@lzu.edu.cn (M.Z. Liu)

View Article Online
DOI: 10.1039/C5RA20996J

biosensor showed great potential applications in the detection of DA with remarkable enhanced effect on voltammetric response of DA. The linear relationship between the response peak currents and DA concentration was in range from 2.0×10^{-9} to 1.0×10^{-5} M, the limits of detection is 6.67×10^{-10} M.. Moreover, the prepared biosensor also showed good selectivity for DA detection in the presence of ascorbic acid and uric acid and satisfactory result in real samples detection.

1.Introduction

Metal-organic frameworks (MOFs), as a new kinds of structured hybrid materials that consist of inorganic connectors and organic linker molecules, have attracted enormous interest because of their large accessible surface areas, high porosity, tunable pore sizes, ordered crystalline structures and excellent mechanical stability.[1-3] These remarkable characteristics helped MOFs showed great potential application in gas adsorption, catalysis, separation and purification.[4] Because many metal ions used in MOFs are electrochemically active, MOFs are also received growing concerns in electrochemical biosensors field.[5,6] To enhance the conductivity, stability in aqueous solution and electro-catalytic activities of target analytes, the introduction of the other highly conductive and mechanically durable materials into MOFs has been proposed.[7,8]

Graphene, composed of a single-atom-thick two-dimensional sheet of covalently bonded carbon atoms, has extraordinary electronic conductivity, high specific surface area, exceptional electron transfer rate, optical, structural and mechanical properties.[9-11] In recent years, the graphene has been pay close attention to be the

View Article Online
DOI: 10.1039/C5RA20996J

outstanding candidate for potential electrode modifying material because its bio-electrocatalytic properties and physical stability.[12, 13] As one kind of chemically derived graphene, reduced graphite oxide (RGO) with similar characteristics to graphene in many aspects has shown great utilization potentiality for application as highly sensitive biosensors.[14] To overcome the poor dispersibility and being prone to aggregation owing to the strong stacking tendency in the synthesis process of bulk-quantity RGO, decorating the RGO nano-sheets with inorganic nanoparticles during the preparation is the reasonable way which not only decreases restacking for RGO nano-sheets but also enhances the physical and chemical properties.[15]

Dopamine (DA) is one of the most significant and representative catecholamine neurotransmitter mediating the transmission of messages within the central nervous system of mammals and humans. An abnormal dopaminergic neuron process may lead to neurological illnesses, such as Parkinson's, Alzheimer's and Schizophrenia diseases.[16] As the trace level concentration of DA change has been related to various diseases, the rapid, sensitive and accurate measurement to detect the trace amount of DA is of extreme importance. Several methods have been established for DA detection, such as liquid chromatography, chemiluminescence, capillary electrophoresis, fluorescence, and absorbance andcolorimetric methods. Because DA can be easily electrochemically oxidized, the electrochemical biosensors have been considered to be superior to other techniques for the determination of DA in view of its high accuracy, fast response, bulk modification with simple instruments, and low operation and instrumental expenses.[17]

View Article Online
DOI: 10.1039/C5RA20996J

Zeolitic imidazolate frameworks (ZIFs) is an attractive subfamily of MOFs due to their exceptional chemical and thermal stabilities and the ease of synthesis. In this work, we have developed a simple method to prepare a novel hybrid nanocomposite of magnetic Fe_3O_4@ZIF-8 decorated graphene with excellent dispersibility and stability in aqueous solution.[18] In this process, Fe_3O_4 decorated RGO is formed firstly by the solvothermal approach, and then ZIF-8 is synthesized on the surface of Fe_3O_4 to get the final products, Fe_3O_4@ZIF-8/RGO nanocomposite. The designed novel structure of anchoring the Fe_3O_4@MOFs nanospheres on graphene nano-sheets could not only restrained restacking of the graphene nano-sheets, but also incorporated of a rapid response towards an assistant magnetic field and fascinating electro-catalytic properties. To explore the potential electrochemical application of the Fe_3O_4@ZIF-8/RGO, the nanocomposite was immobilized on a glassy carbon electrode (GCE) to form a sensing platform for the detection of DA. The results demonstrated that Fe_3O_4@ZIF-8/RGO modified electrode had a high sensitivity, favorable performance and reproducibility, and excellent selectivity for determination of DA.

2. Experiment

2.1. Materials and Reagents

Ferric chloride hexahydrate ($FeCl_3 \cdot 6H_2O$), sodium acetate, ethylene glycol (EG), and $Zn(NO_3)_2 \cdot 6H_2O$ were obtained from Sinopharm Chemical Reagent, Co., Ltd (Shanghai, China). Stock solution of dopamine (0.01 mol L^{-1}) was prepared by dissolving dopamine (0.1531 g) in 100 mL deionized water. The phosphate buffer

View Article Online
DOI: 10.1039/C5RA20996J

solution (PBS, 0.1 mol L^{-1}), which was prepared by mixing Na_2HPO_4 and NaH_2PO_4 stock solution and adjusted to the pH value of 5.0-7.5 with 0.1 mol L^{-1} H_3PO_4 or NaOH solution, was used as the supporting electrolyte during all measurements.

2.2. Apparatus

The FT-IR was recorded with a Nicolet Magna-IR spectrophotometer between 4000 and 450 cm^{-1} using the KBr pellet technique. Transmission electron microscopy (TEM, FEI Tecnai G20) was obtained to elucidate the dimensions of the nanoparticle. The crystalline structures of samples were characterized by X-ray diffraction (XRD) (RigakuD/max-2400). The chemical analysis for the composites were conducted by X-ray photoelectron spectroscopy (XPS, ESCALAB210, VG, UK). Magnetization measurements were performed on a vibrating sample magnetometry (VSM, LAKESHORE-7304, USA). Amperometric measurements were performed on a CHI 660E electrochemical workstation.

2.3. Preparation of Fe_3O_4/RGO nanocomposites

Graphite oxide (GO) was prepared according to the modified Hummers method.[19] Then, Fe_3O_4/RGO nanocomposites were synthesized via the solvothermal approach. Typically, 40 mg of GO was introduced into 30 mL of ethylene glycol (EG) and sonicated for 30 min to get brown dispersion solution. Then 0.987 g of $FeCl_3 \cdot 6H_2O$ and 1.946 g of sodium acetate were dissolved in the EG solution of GO by stirring for 30 min. After that, the mixture was transferred to a Teflon-lined autoclave and treated at 200 ^oC for 8 h. The obtained Fe_3O_4/RGO nanocomposites were collected by magnetic decantation and washed with ethanol and distilled water thoroughly. Finally,

View Article Online
DOI: 10.1039/C5RA20996J

the nanocomposites were dried at 60 ^{o}C of 24 h under vacuum.[20]

2.4. Preparation of Fe_3O_4@ZIF-8/RGO nanocomposites

0.12 g of $Zn(NO_3)_2$ was dissolved in 15 mL of 50% ethanol solution containing 2 mmol HCl. 0.35 g of obtained Fe_3O_4/RGO nanocomposites was dispersed in above solution by sonication for 20 min. After that, 30 mL of 50% ethanol solution containing 0.34 g 2-methylimidazole was added to the suspension and the mixture was stirred with ultrasound at room temperature for 10 min. The product, Fe_3O_4@ZIF-8/RGO nanocomposites, were collected by a magnet and washed with distilled water and ethanol thoroughly, then dried at 60 ^{o}C under the vacuum for 24 h.[21]

2.5. Preparation of Fe_3O_4@ZIF-8/RGO modified electrode

1 mg of Fe_3O_4@ZIF-8/RGO was dispersed in 1 mL of dimethyl formamide (DMF) and the mixture was sonicated for 30 min to achieve a well-dispersed suspension. Prior to modification, the bare GCE was polished to a mirror-like surface sequentially with 1.0, 0.3 mm and 0.05 μm of α-Al_2O_3, and then rinsed ultrasonically with water and ethanol and de-ionized water. After the solvent was evaporated, 5 μL of Fe_3O_4@ZIF-8/RGO suspension was cast onto the electrode surface. Thus the Fe_3O_4@ZIF-8/RGO nanocomposites modified electrode (Fe_3O_4@ZIF-8/RGO/GCE) was obtained after it was dried in air for approximately 3 h. For comparison, the Fe_3O_4@ZIF-8 modified GCE (Fe_3O_4@ZIF-8/GCE) and GO modified GCE (GO/GCE) were prepared only by replacing the Fe_3O_4@ZIF-8/RGO suspension with Fe_3O_4@ ZIF-8 or GO suspension. Fig. 1 shows the preparation of Fe_3O_4@ZIF-8/RGO/GCE

View Article Online
DOI: 10.1039/C5RA20996J

and its application for sensing analysis of DA.

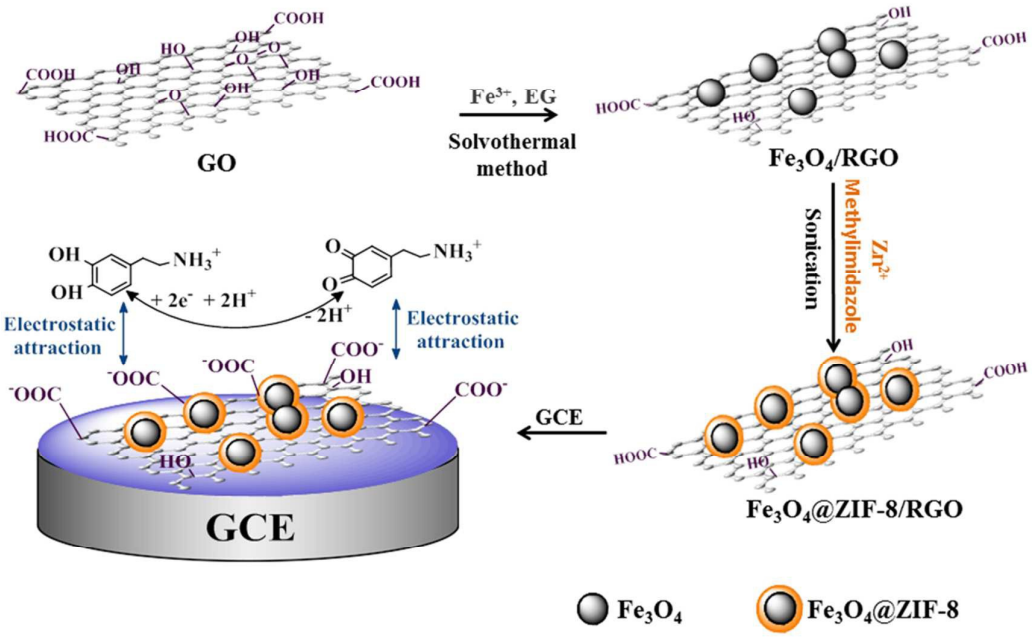

Fig. 1. Scheme for the preparation of Fe_3O_4@ZIF-8/RGO, and its application for the determination of DA.

2.6. Electrochemical measurement

Electrochemical characterizations of the modified electrodes were performed in 0.1 M phosphate buffer solution (PBS) (pH 5.0) through cyclic scan in the potential range from -1.0 to 0.8 V. The electrochemical sensing test of the modified electrode was carried out with a CHI 660E electrochemistry workstation by a conventional three-electrode system, comprising a platinum wire as the auxiliary electrode, a saturated calomel electrode as the reference electrode and the modified GCE as the working electrode in the following procedure: A 15 mL solution containing an appropriate amount of dopamine and 0.1 M PBS was transferred into a voltammetric cell, and then cyclic voltammetry (CV) and differential-pulse voltammetry (DPV) measurements were recorded. Real samples determination was experimented by the

View Article Online
DOI: 10.1039/C5RA20996J

standard addition method. The urine and serum samples were diluted with PBS (0.1 M, pH 5.5) and spiked with different amounts of known concentrations of DA, and measured under the optimal conditions.

3. Results and discussion

3.1. Characterization of Fe_3O_4@ZIF-8/RGO nanocomposites

The morphologies of the Fe_3O_4/RGO, Fe_3O_4@ZIF-8 and Fe_3O_4@ZIF-8/RGO are characterized by SEM and TEM, and the TEM and SEM images of each synthesized composites are shown in Fig. 2. As shown in Fig. 2a and d, Fe_3O_4 nanoparticles have been decorated on the surface of graphene nano-sheets with a diameter of about 200 nm. The monodisperse core-shell structure of Fe_3O_4@ZIF-8 is just like the reported.[21] The nearly spherical shape of Fe_3O_4@ZIF-8 and the formation of the ZIF-8 shell could be observed by the SEM image (Fig. 2b) and TEM image (Fig. 2e). Compared with Fe_3O_4/RGO and Fe_3O_4@ZIF-8, the Fe_3O_4@ZIF-8/RGO nanocomposites (Fig. 2c and f) combined two features of each composites, the folds of graphene sheets and core-shell structure of Fe_3O_4@ZIF-8 are exhibited obviously in the images. Therefore, demonstrated by TEM and SEM results, the novel Fe_3O_4@ZIF-8/RGO nanocomposites have been successfully prepared.

View Article Online
DOI: 10.1039/C5RA20996J

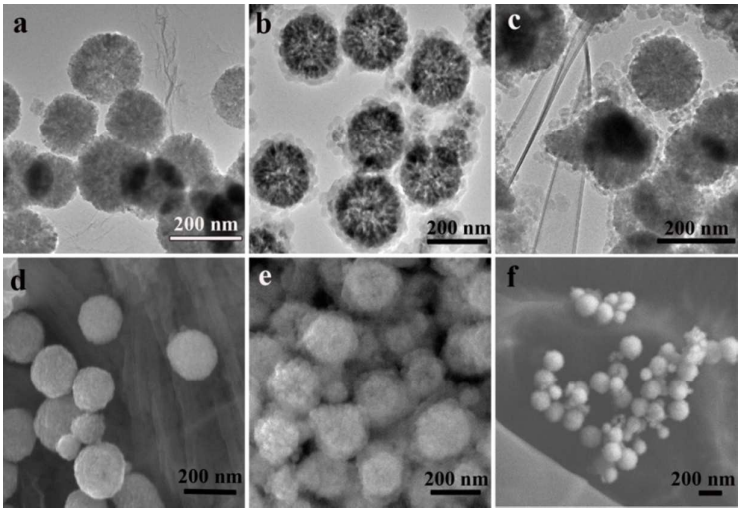

Fig. 2. TEM images of the Fe_3O_4/RGO (a), Fe_3O_4@ZIF-8 (b) and Fe_3O_4@ZIF-8/RGO (c) and SEM images of the Fe_3O_4/RGO (d), Fe_3O_4@ZIF-8 (e) and Fe_3O_4@ZIF-8/RGO (f)

The chemical structures of the Fe_3O_4, Fe_3O_4/RGO, Fe_3O_4@ZIF-8 and Fe_3O_4@ZIF-8/RGO are characterized by FT-IR spectra, as presented in Fig. 3. The spectrum of Fe_3O_4 is just same to the report, and the peak at 580 cm^{-1} is related to the vibration of Fe-O functional groups.[22] While in the FT-IR spectrum of Fe_3O_4/RGO, the bands at 3490 cm^{-1} and 1200cm^{-1} appear, which correspond to the stretching vibration of C-H and C-N (in the -C-NH-C- group), respectively.[23, 24] Compared to the spectrum of Fe_3O_4, the spectrum of Fe_3O_4@ZIF-8 displays different peaks contributed by the ZIF-8 shell. The bands in region of 900-1330 cm^{-1} and band at 1440 cm^{-1} are attributed to the imidazole ring, and the band at 422 cm^{-1} could be assigned to the Zn-N stretch mode.[21, 25] The spectrum of Fe_3O_4@ZIF-8/RGO nanocomposites also combines the features of above composites, and shows the characteristic absorption bands of each constituent part. Overall, the FT-IR spectra confirmed the formation of Fe_3O_4@ZIF-8/RGO structure.

View Article Online
DOI: 10.1039/C5RA20996J

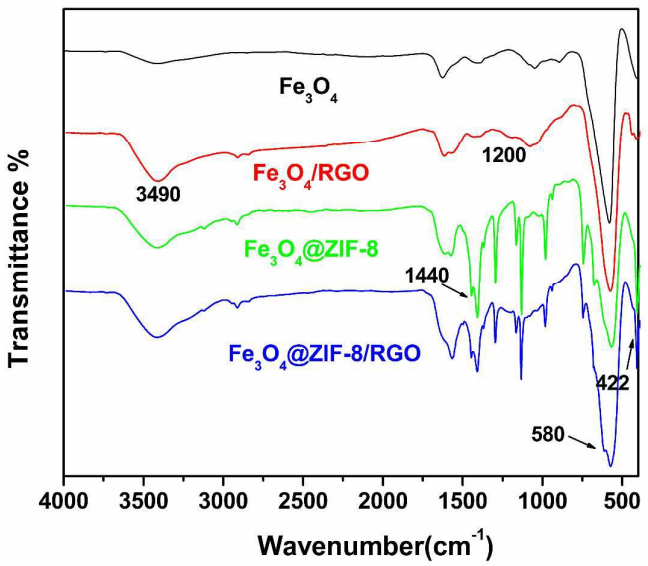

Fig. 3. FT-IR spectrum of Fe_3O_4, Fe_3O_4@ZIF-8, Fe_3O_4/RGO and Fe_3O_4@ZIF-8/RGO nanocomposite

The crystal structure of the as prepared samples have been identified by X-ray power diffraction techniques and the XRD spectrum are show in Fig. 4. The intense and sharp peak at 10.6° in the spectrum of GO is attributed to the crystalline plane of graphite oxide, and the diffraction peaks of Fe_3O_4 can be assigned to a superposition of standard XRD pattern of face-centered cubic Fe_3O_4.[26] However, the peak at 10.6° has entirely disappeared after the Fe_3O_4 decorated on the graphene through hydrothermal reaction because EG could reduce GO and Fe^{3+} to graphene and Fe^{2+}, repectively.[20, 27] Simultaneously, standard Fe_3O_4 XRD pattern in the spectrum of Fe_3O_4/RGO demonstrating the Fe_3O_4 nanoparticles are successfully decorated on graphene sheets. The XRD pattern of Fe_3O_4@ZIF-8 is consistent with the characteristic peaks of Fe_3O_4 and the simulated pattern of published ZIF-8 structure data.[21, 28] The diffraction peaks of Fe_3O_4@ZIF-8/RGO are very similar to Fe_3O_4@ZIF-8, indicating the coexistence of Fe_3O_4@ZIF-8 and graphene in the

View Article Online
DOI: 10.1039/C5RA20996J

resulted nanocomposite.

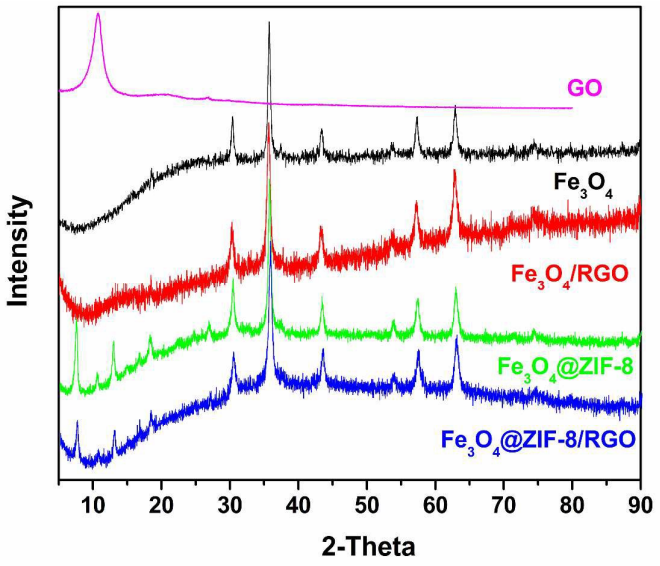

Fig. 4. XRD spectrum of Fe_3O_4, Fe_3O_4@ZIF-8, Fe_3O_4/RGO and Fe_3O_4@ZIF-8/RGO nanocomposite

To investigate the chemical elements on the surface of the Fe_3O_4/RGO and Fe_3O_4@ZIF-8/RGO, the XPS analysis was performed. The wide-scan XPS spectra for Fe_3O_4/RGO and Fe_3O_4@ZIF-8/RGO are shown in Fig. 5(a). The characteristic peaks of Fe 2p, Fe 3p, O 1s and C 1s appeared in the spectrum of Fe_3O_4/RGO. Compared with the Fe_3O_4/RGO, new peaks assigned to Zn 2p1, Zn 2p3 and N 1s are clearly observed in the spectrum of Fe_3O_4@ZIF-8/RGO, demonstrated the MOFs (ZIF-8) have been successfully reacted on the surface of Fe_3O_4. Moreover, as the ZIF-8 was covered on the Fe_3O_4, the peaks of Fe 2p and Fe 3p are disappeared and the peak of O 1s decreased sharply. Fig. 5(b) shows the C 1s spectrums of Fe_3O_4/RGO and Fe_3O_4@ZIF-8/RGO, the only peak at 527.95 eV could be assigned to the C-C in the spectrum of Fe_3O_4/RGO, and two peaks in Fe_3O_4@ZIF-8/RGO corresponding to C-C (183.51 eV) and C=C (186.16 eV) demonstrated the 2-methylimidazole has covered

View Article Online
DOI: 10.1039/C5RA20996J

on the Fe_3O_4. The N 1s spectrum of Fe_3O_4@ZIF-8/RGO (Fig. 6(c)) shows two species of N 1s peak corresponding to -NH- (397.53 eV) and –N= (400.59 eV) which also characterized the 2-methylimidazole on the nanocomposite.[20, 29]

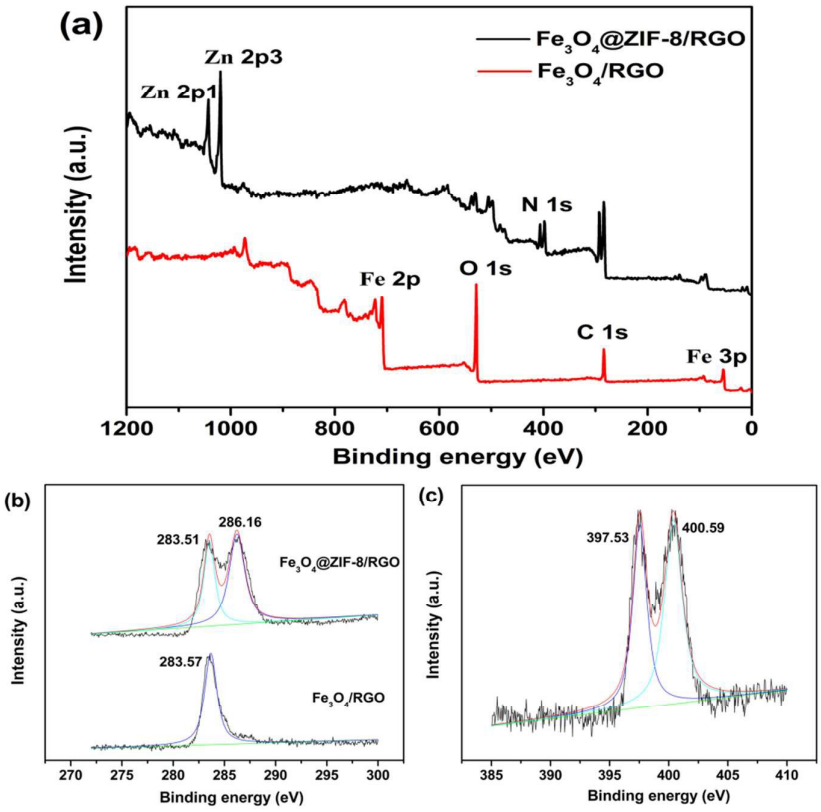

Fig. 5. XPS spectra of (a) wide scan of Fe_3O_4/RGO and Fe_3O_4@ZIF-8/RGO; (b) N 1s of Fe_3O_4@ZIF-8/RGO; (c) C1s of Fe_3O_4/RGO and Fe_3O_4@ZIF-8/RGO

The magnetic property of Fe_3O_4@ZIF-8/RGO was studied using a superconducting quantum interference device (SQUID) magnetometer at room temperature, as shown in Fig. 6. The hysteresis loops of the Fe_3O_4 nanoparticle, Fe_3O_4/RGO, Fe_3O_4@ZIF-8 and Fe_3O_4@ZIF-8/RGO nanocomposite are characterized the magnetic measurements of each product. The saturation magnetization of Fe_3O_4, Fe_3O_4/RGO, Fe_3O_4@ZIF-8 and Fe_3O_4@ZIF-8/RGO is 79.08, 60.87, 50.41 and 41.65 emu g^{-1}, respectively. Although the magnetic intensity of Fe_3O_4@ZIF-8/RGO decreases obviously after the

View Article Online
DOI: 10.1039/C5RA20996J

ZIF-8 was reacted on the Fe_3O_4, the Fe_3O_4@ZIF-8/RGO nanocomposite can be easily separated conveniently by using magnetic field, and facilitated collection and operation.[30]

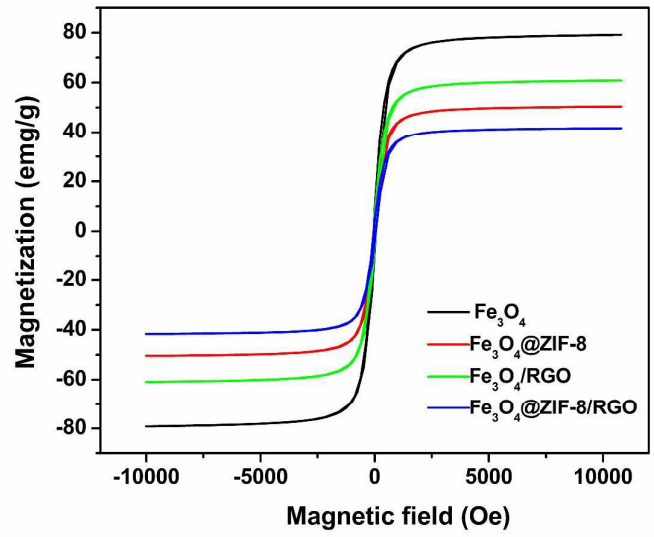

Fig. 6. VSM curves (B) of Fe_3O_4, Fe_3O_4@ZIF, Fe_3O_4/RGO and Fe_3O_4@ZIF-8/RGO nanocomposite

3.2. Voltammetric behavior of DA at Fe_3O_4@ZIF-8/RGO/GCE

To exploit the potential application of the Fe_3O_4@ZIF-8/RGO nanocomposite, the electrochemical behaviors of DA were investigated on the Fe_3O_4@ZIF-8/RGO /GCE. Fig. 7 shows typical CVs of 1 mM DA on the bare GCE, the Fe_3O_4@ZIF-8 /GCE, the Fe_3O_4/RGO/GCE and the Fe_3O_4@ZIF-8/RGO/GCE. On the bare GCE, DA exhibits a reversible electrochemical behavior and the small current indicates it is inefficient to detect of DA on the bare GCE. At the Fe_3O_4@ZIF-8, a couple of small redox peaks appeared and the oxidation peak current of DA enhanced notable, it is because that the relative large surface area of electrode increased significantly after immobilization of Fe_3O_4@ZIF-8. Due to the excellent electric conductivity of reduced

View Article Online
DOI: 10.1039/C5RA20996J

graphite oxide, the anodic peak current at the Fe_3O_4/RGO/GCE is increased strikingly. However, when the Fe_3O_4@ZIF-8/RGO/GCE was applied for determination, the redox peaks of DA increased dramatically with a well-defined peak shape, and the redox process became more reversible as judged from the more symmetric peak profiles. Therefore, the component of MOFs (ZIF-8) material in the graphene nano-sheets have positive effect on improving the electrochemical response, which is likely caused by the outstanding porous structure and favorable electron transfer mediating function of the electroactive MOFs.[7, 31]

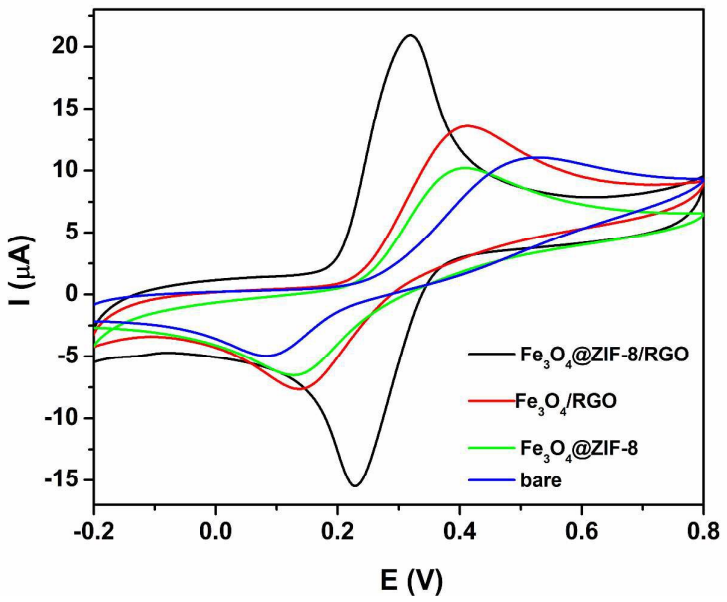

Fig. 7. Cyclic voltammograms at the are GCE, the Fe_3O_4@ZIF-8 /GCE, the Fe_3O_4/RGO/GCE and the Fe_3O_4@ZIF-8/RGO/GCE in the presence of DA in PBS (0.1M, pH 5.5). DA concentration: 1 mM, and scan rate: 20 mV s^{-1}

3.3. Electrochemical parameters of DA at Fe_3O_4@ZIF-8/RGO/GCE

The influence of the scan rate (ν) on the oxidation current of 0.1 mM DA was examined using Fe_3O_4@ZIF-8/RGO/GCE in 0.1 M pH 5.0 PBS by varying the scan

View Article Online
DOI: 10.1039/C5RA20996J

rates from 10 to 50 mV s^{-1}. As shown in Fig. 8, the anodic and cathodic peak currents are both increased gradually when increasing the scan rate. Farther more, with the increase of scan rate, the anodic peak potential and cathodic peak potential slightly shifted to more positive and negative potentials, respectively, indicating that the electrontransfer rate decreased and the electrochemical reaction of DA tended to be less reversible. A good linear relationship among the scan rate, the values of the anodic peak current (I_{pa}) and the cathodic peak current (I_{pc}) is also obtained. The linear regression equation for the anodic peak current and cathodic current is I_{pa} (μA) = 5.6328 + 0.21468ν (mV s^{-1}), and I_{pc} (μA) = -3.1756 - 0.1023ν (mV s^{-1}), respectively, and the correlation coefficient is R_{pa} = 0.9965, R_{pc} = 0.9903, respectively. This result suggests that the electrochemical oxidation is an absorption-controlled process for DA at the Fe_3O_4@ZIF-8/RGO/GCE surface.[32]

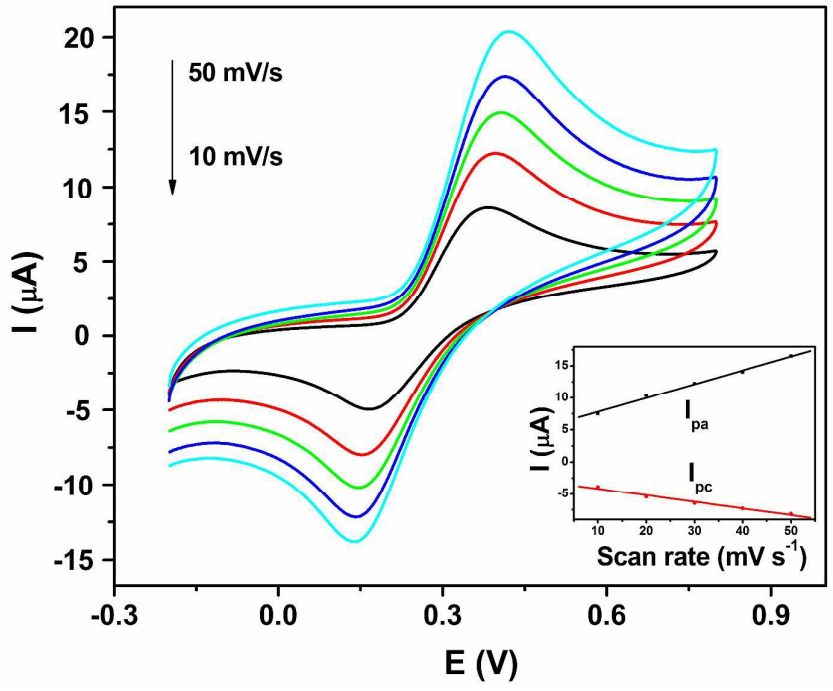

Fig. 8. Cyclic voltammograms of 0.1 mM DA in 0.1 mM PBA at the

View Article Online
DOI: 10.1039/C5RA20996J

Fe_3O_4@ZIF-8/RGO/GCE at scan rate of 10-50 mV s^{-1}. The inset shows the plots of anodic and cathodic peak currents *vs.* scan rates.

Since the redox system was affected by the change of pH due to the involvement of protons in the electrode reaction and the electro-catalytic reaction at the Fe_3O_4@ZIF-8/RGO/GCE is a two electron, two proton process, the influence of pH on the biosensor performance was investigated by measuring the electrode response in 0.1 mM DA with pH values ranging from 5.0 to 7.5. [33] As shown in Fig. 9, the oxidation peak potential (E_{pa}) of DA shifted negatively with the increased of pH. A good linear relationship between E_{pa} and pH was constructed and described with a linear equation: E(V) = -0.0704 pH + 0.7773 (R=0.9935). Farther more, the oxidation peak current (I_{pa}) also changed with the pH of DA solution ranged from 5.0 to 7.5, and the maximum response current was obtained at pH of 5.5. Thus, a phosphate buffer solution of pH 5.5 was chosen as the optimum pH and used in all experiments below.

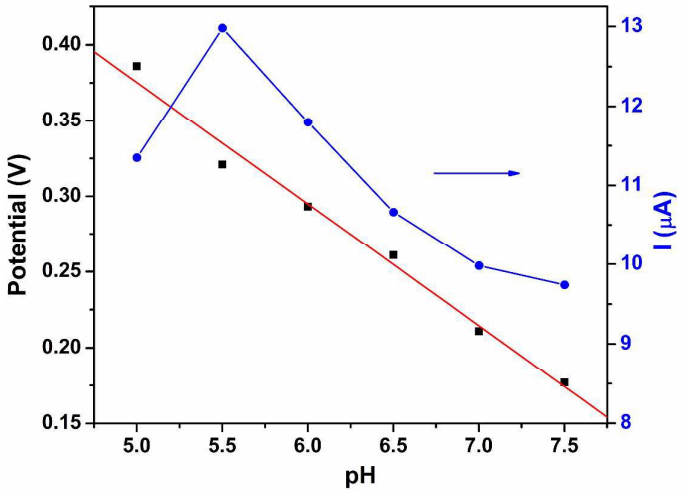

Fig. 9. Effects of pH on E_{pa} and I_{pa} of 0.1 mM in 0.1 M PBS on the Fe_3O_4@ZIF-8/RGO/GCE

View Article Online
DOI: 10.1039/C5RA20996J

3.4. Analytical performance and applications

Voltammetric current responses of successive additions of DA were recorded by differential pulse voltammetry (DPV) to check the sensitivity of the sensor under the optimal experimental conditions. As shown in Fig. 10, with the increasing concentration of DA, the oxidation peak current (I_{pa}) increased relatively. Linearly proportional of peak current and DA concentration is observed in the range from 2.0×10^{-9} to 1.0×10^{-5} M (inset of Fig. 10). The linear regression equations for DA is I_{pa} (μA) = 1.144 + 0.0056C (10^{-9} M) and the correlation coefficient is 0.9966. According to signal to noise (S/N) = 3, the detection limits of DA was estimated to be 6.67×10^{-10} M. Table 1 summarized the comparison of analytical results of the analytical performance Fe_3O_4@ZIF-8/RGO/GCE with other dopamine sensor reported recently. Through the comparison, the obtained biosensor in this work has comparable and even better performance than the others, demonstrating that Fe_3O_4@ZIF-8/RGO/GCE has extraordinary application potential in determination of DA.

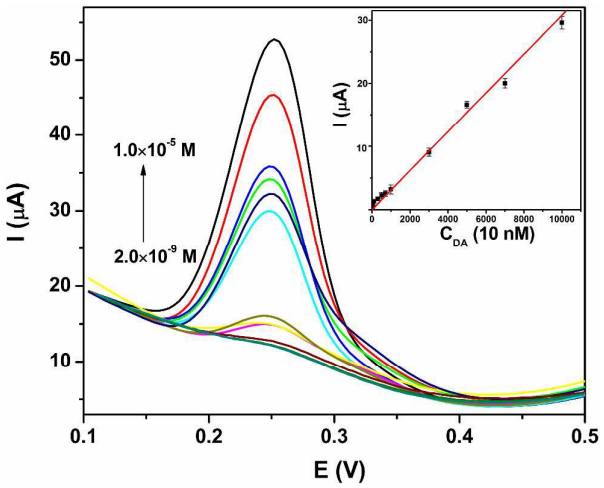

Fig. 10. DPV for different concentration of DA at the Fe_3O_4@ZIF-8/RGO/GCE. The inset shows the relationship between the peak current and DA concentration

View Article Online
DOI: 10.1039/C5RA20996J

Table 1 Comparison of analytical performance of DA at different modified electrodes

Modified materials	Methods	Linear ranges (M)	Detection limits (M)	reference
GO	DPV	1×10^{-6}-1.5×10^{-7}	0.27×10^{-6}	35
Fe_3O_4/r-GO	DPV	4×10^{-7}-1.6×10^{-4}	8×10^{-8}	36
Pd/graphene/chitosan	DPV	5×10^{-7}-2×10^{-4}	1×10^{-7}	37
Polypyrrole@r-GO	DPV	6×10^{-8}-8×10^{-6}	6×10^{-9}	38
Cu(tpa)-EGR	DPV	1×10^{-6}-5×10^{-5}	2.1×10^{-7}	7
Nafion/C/Al-MIL-53-$(OH)_2$	DPV	3×10^{-8}-1×10^{-5}	8×10^{-9}	8
Porphyrin-RGO	DPV	1×10^{-6}-7×10^{-5}	9.5×10^{-9}	39
RGO-MWNTs-PTA	DPV	5×10^{-7}-2×10^{-5}	1.14×10^{-6}	40
Fe_3O_4@ZIF-8/RGO	DPV	2×10^{-9}- 1×10^{-5}	6.67×10^{-10}	This work

As an important parameter for a biosensor, discriminating the target between the interfering species in similar physiological environments is necessary to be investigated. For the determination of DA, the electrochemical behaviors of ascorbic acid (AA), and uric acid (UA) (usually coexist with DA) on Fe_3O_4@ZIF-8/RGO/GCE has be studied. As shown in Fig. 11, a couple of shape redox peaks is exhibited in the CV of 1 mM of DA, on the contrary, no obvious peak appeared in the CV of 1×10^{-3} M of AA and UA, which suggested that DA can be detected in the presence of AA and UA.[34] To demonstrate the selectivity of Fe_3O_4@ZIF-8/RGO/GCE for DA more comprehensively, various potential organic compounds and inorganic ions such as NaCl, K_2SO_4, $CaCl_2$ solutions, lysine, cysteine and glucose solutions were added to the 1 mM of DA solution. The peak currents of DA showed almost no interference in the presence of these influences since their peak currents changes were below 5%. A possible reaction mechanism was discussed here, the negatively charged Fe_3O_4@ZIF-8/RGO acted as electro-catalysts and selective reagents simultaneously,

View Article Online
DOI: 10.1039/C5RA20996J

thus, the positively charged DA was attracted and electro-catalyzed on the sensor, otherwise, the negatively charged analytes such as AA and UA were repelled. Therefore, with a wide linear range, low detection potential, and high sensitivity, the Fe_3O_4@ZIF-8/RGO could be used as promising candidates to prepare the dopamine biosensors.

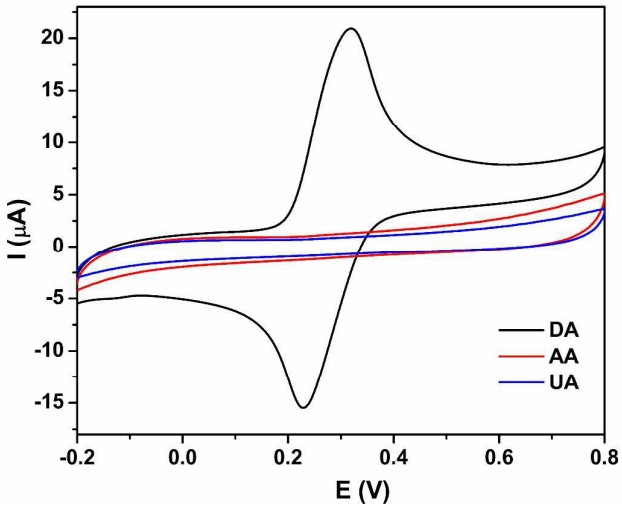

Fig. 11. Cyclic voltammograms of the Fe_3O_4@ZIF-8/RGO/GCE in 0.1 PBS with 1 mM DA, AA and UA, respectively.

3.5. Reproducibility of biosensor and real sample determination.

The reproducibility and stability of the Fe_3O_4@ZIF-8/RGO/GCE were further examined. When the electrode was successively scanned in 1 mM DA in 0.1 M pH 5.0 PBS for 50 cycles, there were no obvious changes in the peak current in the CV curves. Repeated DPV experiment was also conducted in the same condition, and the relative standard deviation (RSD) was 2.13% after 15 successive measurements. The long-term stability of the electrode was investigated by measuring its CV response over a 10 day period. The fabricated electrodes were stored under normal conditions at room temperature, and no obvious changes were found when measured it

View Article Online
DOI: 10.1039/C5RA20996J

periodically. Therefore, the results indicated the excellent reproducibility and stability of the prepared Fe_3O_4@ZIF-8/RGO/GCE biosensor. Real samples were analyzed by the standard addition method to evaluate the potential application of Fe_3O_4@ZIF-8/RGO/GCE biosensor. Urine and serum samples were diluted with PBS (0.1 M, pH 5.5) in order to avoid the interferences of the complicated matrix in the real samples and fit into the linear ranges of DA. Then the diluted samples were spiked with different amounts of known concentrations of DA, and measured under the optimal conditions. The analytical results are shown in Table 2. As can be observed, the recovery of the spiked samples was in the range of 98.20-102.73% (n = 5) with the relative standard derivation (RSD) values were calculated to be less than 2.69%, indicated that the method is reliable and sensitive for determination of DA in real samples.

Table 2 Determination of DA in real samples using Fe_3O_4@ZIF-8/RGO/GCE

Samples	Added (μM)	Found (μM)	RSD (%)	Recovery (%)
Serum 1	—	0.093	1.91	—
	0.200	0.301	2.23	102.73
	0.500	0.597	2.54	100.81
Serum 2	—	0.223	2.36	—
	0.200	0.429	1.87	101.42
	0.500	0.719	1.61	99.44
Urine 1	—	0.134	2.62	—
	0.200	0.328	2.69	98.20
	0.500	0.639	2.28	100.88
Urine 2	—	1.102	1.77	—
	0.200	1.309	1.89	100.73
	0.500	1.597	2.01	99.61

4. Conclusions

In this paper, a novel hybrid nanocomposite of magnetic Fe_3O_4@ZIF-8 decorated

View Article Online
DOI: 10.1039/C5RA20996J

graphene was prepared by a simple method for the first time. After the Fe_3O_4/RGO was formed by solvothermal approach, the MOFs (ZIF-8) was fabricated on the surface of Fe_3O_4 to get the Fe_3O_4@ZIF-8/RGO nanocomposite. By combing the unique properties of large specific surface area and high conductivity derived from both of MOFs and graphene, the Fe_3O_4@ZIF-8/RGO nanocomposites modified glassy carbon electrode was successfully constructed and used for electrochemical detection of DA. The fabricated biosensor showed great potential applications in the detection of DA with extraordinary advantages such as wide linear range (2.0×10^{-9}–1.0×10^{-5} M), low detection limit (6.67×10^{-10}) and good selectivity for DA detection in the presence of ascorbic acid and uric acid. Moreover, the prepared sensor also showed satisfactory result in real samples detection. Our present study demonstrated the combination of MOFs and graphene composites could fabricate a new kind of high sensitive biosensor for electrochemical detection.

Acknowledgments

The authors gratefully acknowledge financial supports from the National Natural Science Foundation of China (No. 21304040), Natural Science Foundation of Gansu Province (1308RJYA027) and Chinese Postdoctoral Funds (2013M532090). This paper is dedicated to memory of pro. Yanfeng Li, who passed away recently.

View Article Online
DOI: 10.1039/C5RA20996J

Reference

1 J. R. Li, J. Sculley and H. C. Zhou, *Chem. Rev*., 2011, **112**, 869.

2 M. Yaghi, M. O'Keeffe, N. W. Ockwig, H. K. Chae, M. Eddaoudi and J. Kim, *Nature*, 2003, **423**, 705.

3 P. Chowdhury, C. Bikkina, D. Meister, F. Dreisbach and S. Gumma, *Microporous Mesoporous Mater*., 2009, **117**, 406.

4 M. Zhao, S. Ou and C. D. Wu, *Acc. Chem. Res*., 2014, **47**, 1199.

5 Y. Li, C. Huangfu, H. Du, W. Liu, Y. Li and J. Ye, *J. Electroanal. Chem*., 2013, **709**, 65.

6 Y. Zhang, X. Bo, C. Luhana, H. Wang, M. Li and L. Guo, *Chem. Commun*., 2013, **49**, 6885.

7 X. Wang, Q. X. Wang, Q. H. Wang, F. Gao, F. Gao, Y. Z. Yang and H. X. Guo, *ACS Appl. Mat. Interfaces*, 2014, **6**, 11573.

8 Y. Wang, H. L. Ge, G. Q. Ye, H. H. Chen and X. Y. Hu, *J. Mater. Chem. B*, 2015, **3**, 3747.

9. X. Li, S. Zhu, B. Xu, K. Ma, J. Zhang, B. Yang and W. Tian, *Nanoscale*, 2013, **5**, 7776.

10. L. Li, A. R. O. Raji and J. M. Tour, *Adv. Mater*., 2013, **25**, 6298.

11 B. Zhan, C. Liu, H. Chen, H. Shi, L. Wang, P. Chen, W. Huang and X. Dong, *Nanoscale*, 2014, **6**, 7424.

12 C. Z. Liao, M. Zhang, L. Y. Niu, Z. j. Zheng and F. Yan, *J. Mater. Chem. B*, 2014, **2**, 191-200.

13 X. M. Feng, Y. Zhang, J. h. Zhou, Y. Li, S. F. Chen, L. Zhang, Y. W. Ma, L. H. Wang and X. H. Yan, *Nanoscale*, 2015, **7**, 2427.

14 A. M. J. Haque, H. Park, D. Sung, S. Jon, S. Y. Choi and K. Kim, *Anal. Chem.*, 2012, **84**, 1871.

15 X. H. Li, H. Zhu, J. Feng, J. Zhang, X. Deng, B. Zhou, H. Zhang, D. Xue, F. Li, N. Mellors, Y. F. Li and Y. Peng, *carbon*, 2013, **60**, 488.

View Article Online
DOI: 10.1039/C5RA20996J

16 S. Ikemoto, *Brain Res. Rev*., 2007, **56**, 27.

17 W. X. Zhang, J. Z. Zheng, C. H. Tan, X. Lin, Sh. R. Hu, J. H. Chen, X. L. You and S. X. Li, *J. Mater. Chem. B*, 2015, **3**, 217-224.

18 Y. C. Pan, Y. Y. Liu, G. F. Zeng, L. Zhao and Z. P. Lai, *Chem. Commun*., 2011, **47**, 2071.

19 H. Zhou, W. Yao, G. Li, J. Wang and Y. Lu, *Carbon*, 2013, **59**, 495.

20 W. Yao, T. Ni, S. Chen , H. Li and Y. Lu, *Compos. Sci. Technol*., 2014, **99**, 15.

21 J. N. Zheng, Z. Lin, G. Lin, H. H. Yang and L. Zhang, *J. Mater. Chem. B*, 2015, **3**, 2185.

22 Y. Wang, Y. Zhang, C. Hou, Z. Qi, X. He, *Chemosphere*, 2015, **141**, 26.

23 Y. Q. Wang, B. F. Zou, T. Gao, X. P. Wu, S. Y. Lou, S. M. J. Zhou, *Mater. Chem*., 2012, **22**, 9034.

24 H. L. Ma, Y. W. Zhang, Q. H. Hu, D. Yan, Z. Z. Yu, Zhai M. L. Zhai, *J. Mater. Chem*., 2012, **22**, 5914.

25 Y. Hu, H. Kazemian, S. Rohani, Y. N. Huang and Y. Song, *Chem. Commun*., 2011, **47**, 12694.

26 W. Fan, W. Gao, C. Zhang, W. W. Tjiu, J. S. Pan, T. X. Liu, *J. Mater. Chem*., 2012, **22**, 25108.

27 K. F. Zhou, Y. H. Zhu, X. L. Yang, C. Z. Li, *New J. Chem.*, 2010, **34**, 2950.

28 K. S. Park, Z. Ni, A. P. Côté, J. Y. Choi, R. Huang, F. J. Uribe-Romo, H. K. Chae, M. O'Keeffe and O. M. Yaghi, *Proc. Natl. Acad. Sci. U. S. A.*, 2006, **103**, 10186.

29 L. Sun, L. Wang, C. G. Tian, T. X. Tan, Y. Xie and K. Y. Shi, *RSC Adv.*, 2012, **2**, 4498.

30 Y. Wang, Y. Zhang, C. Hou, X. He, M. Liu, *J. Taiwan Inst. Chen. E.,* 2015, doi:10.1016/j.jtice.2015.05.044.

31 C. L. Sun, H. H. Lee, J. M. Yang and C. C. Wu, *Biosens. Bioelectron*., 2011, **26**, 3450.

32 M. Zheng, F. Gao, Q. Wang, X. Cai, S. Jiang, L. Huang and F. Gao, *Mater. Sci. Eng*. C, 2013,

View Article Online
DOI: 10.1039/C5RA20996J

33, 1514.

33 J. Yang, J. R. Strickler and S. Gunasekaran, *Nanoscale*, 2012, **4**, 4594.

34 X. Dong, X. Wang, L. Wang, H. Song, H. Zhang, W. Huang and P. Chen, *ACS Appl. Mat. Interfaces*, 2012, **4**, 3129.

35 F. Gao, X. Cai, X. Wang, C. Gao, S. Liu, F. Gao and Q. Wang, *Sens. Actuators, B*, 2013, **186**, 380.

36 H. Teymourian, A. Salimi and S. Khezrian, *Biosens. Bioelectron*., 2013, **49**, 1.

37 X. Wang, M. Wu, W. Tang, Y. Zhu, L. W. Wang, Q. J. Wang, P. J. He and Y. Z. Fang, *J. Electroanal. Chem*., 2013, **695**, 10.

38 T. Qian, S. S. Wu and J. Shen, *Chem. Commun*., 2013, **49**, 4610.

39 S. F. Hou, M. L. Kasner, S. J. Su, K. Patel and R. Cuellari, *J. Phys. Chem.*, 2010, **114**, 14915.

40 Y. Y. Ling, Q. A. Huang, M. S. Zhu, D. X. Feng, X. Z. Li and Y. J. Wei, *Electroanal. Chem*., 2013, **693**, 9.

View Article Online
DOI: 10.1039/C5RA20996J

Graphical abstract:

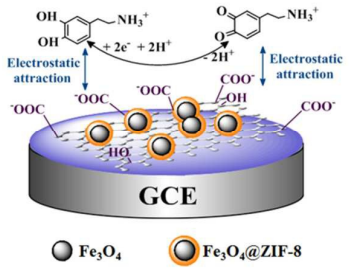

A novel hybrid nanocomposite of magnetic Fe_3O_4@ZIF-8 decorated reduced graphite was prepared and used to determination of dopamine.